Bloch–Kohn and Wannier–Kohn functions inone dimension

2003 J. Phys.: Condens. Matter 15 6701

(http://iopscience.iop.org/0953-8984/15/40/008)

INSTITUTE OF PHYSICS PUBLISHING JOURNAL OF PHYSICS: CONDENSED MATTER

J. Phys.: Condens. Matter **15** (2003) 6701–6714 PII: S0953-8984(03)63454-5

Bloch–Kohn and Wannier–Kohn functions in one dimension

Alexys Bruno-Alfonso[1] **and Guo-Qiang Hai**[2]

[1] Departamento de Matemática, Faculdade de Ciências, Universidade Estadual Paulista, Avenida Luis Edmundo Carrijo Coube sn, 17033-360, Bauru-SP, Brazil
[2] Instituto de Física de São Carlos, Universidade de São Paulo, 13560-970, São Carlos- SP, Brazil

E-mail: alexys@fc.unesp.br

Received 12 May 2003, in final form 22 August 2003
Published 26 September 2003
Online at stacks.iop.org/JPhysCM/15/6701

Abstract

Bloch and Wannier functions of the Kohn type for a quite general one-dimensional Hamiltonian with inversion symmetry are studied. Important clarifications on null minigaps and the symmetry of those functions are given, with emphasis on the Kronig–Penney model. The lack of a general selection rule on the miniband index for optical transitions between edge states in semiconductor superlattices is discussed. A direct method for the calculation of Wannier–Kohn functions is presented.

1. Introduction

Bloch functions (BFs) and Wannier functions (WFs) play a central role in solid state physics, and their properties have been studied in some detail [1–3]. While BFs describe extended electron stationary states, WFs represent localized states obtained by a unitary transformation of BFs. The growing interest in WFs is due to their application in order-N methods for electronic structure calculations and spontaneous polarization studies [4], for example. At the same time, the realization of semiconductor superlattices (SLs) has impelled the study of electron states in one-dimensional (1D) crystals [5]. Localized states such as Wannier–Stark and Landau states, electron–photon and electron–phonon processes may be described in terms of WFs in SLs [6]. However, some misunderstandings regarding the symmetry of miniband-edge BFs, null minigaps (NMGs) and the calculation of exponentially localized WFs are found in the recent literature [7–9]. Therefore, further analysis is needed for a better description of optical properties in SLs, for instance [10].

For the jth miniband (MB) of a 1D crystal of period τ in the x-axis, the BF $\psi_{j,k}(x)$ of wavenumber k (with $-\pi/\tau < k \leqslant \pi/\tau$) satisfies $\psi_{j,k}(x+\tau) = \exp(\mathrm{i}k\tau)\psi_{j,k}(x)$, and the WF of the nth site is obtained as $w_{j,n}(x) = w_j(x - n\tau)$, with

$$w_j(x) = \sqrt{\frac{\tau}{2\pi}} \int_{-\pi/\tau}^{\pi/\tau} \psi_{j,k}(x)\,\mathrm{d}k. \tag{1}$$

0953-8984/03/406701+14$30.00

As BFs are determined up to a k-dependent phase factor, equation (1) shows clearly that $w_j(x)$ is not unique. For a simple MB of a system with an inversion centre at $x = 0$, Kohn [2] has shown that BFs may be chosen to give a real, even or odd about either $x = 0$ or $\tau/2$, and exponentially localized $w_j(x)$. Such a function and its periodic images $w_j(x - n\tau)$ are the Wannier–Kohn functions (WKFs) [11], and the corresponding BFs are called as Bloch–Kohn functions (BKFs). Moreover, four MB classes are considered [2, 12] with regard to the parity of $\psi_{j,0}(x)$ and $\psi_{j,\pi/\tau}(x)$ about $x = 0$ and $\tau/2$.

In this work we address four important questions on the properties of Bloch states and WFs for a 1D crystal with an inversion centre at $x = 0$. First, $\psi_{j,0}(x)$ and $\psi_{j,\pi/\tau}(x)$ have definite parity about $x = 0$. Does the parity of $\psi_{j,0}(x)$ alternate between even and odd as j increases? What about the parity of $\psi_{j,\pi/\tau}(x)$? It should be noted that an alternation of parities has been claimed for the Kronig–Penney (KP) model [7] and has been expected for conduction envelope functions in SLs [10]. Second, NMGs are known to be relevant in the study of transport and optical phenomena in SLs [13, 14]. How do we determine the system parameters leading to NMGs? Third, $\psi_k(x)$ has no definite parity for $0 < k < \pi/\tau$ in general, and its degree of parity mixing has been studied [15]. How do we determine the effective parity of $\psi_{j,k}(x)$? Fourth, may we establish a direct procedure to obtain WKFs?

We show that the parity of $\psi_{j,0}(x)$ does not alternate with increasing j, neither in general nor for the KP model. Instead, the parity sequence depends on the 1D crystal parameters. The same thing applies to $\psi_{j,\pi/\tau}(x)$. Equations leading to MB edges corresponding to a given symmetry are set, thus allowing the classification of MBs and WKFs. We derive conditions on NMGs, and show that minigap-edge BFs may swap their parities when the minigap vanishes and reopens as crystal parameters are continuously varied. Hence, the lack of a general sequence for the parity of $\psi_{j,0}(x)$ (or $\psi_{j,\pi/\tau}(x)$) is explained. We show that, depending on the MB class, BKFs are obtained by choosing $\psi_k(0)$, $\psi_k'(0)$, $\psi_k(\tau/2)$ or $\psi_k'(\tau/2)$ as positive. Then, an algorithm to obtain BKFs within the transfer matrix technique is given. We introduce the effective parity of $\psi_k(x)$ and discuss its main properties. Finally, the theory is applied to the KP model and relevant clarifications on BKFs, WKFs and optical transitions in SLs are made.

2. The Hamiltonian and transfer matrix

The 1D Hamiltonian is written as

$$\hat{H} = -\frac{\hbar^2}{2}\frac{\mathrm{d}}{\mathrm{d}x}\frac{1}{m^*(x)}\frac{\mathrm{d}}{\mathrm{d}x} + V(x), \tag{2}$$

where $V(x)$ and $m^*(x)$ are the effective potential and the longitudinal effective mass respectively. Such functions are supposed to be piecewise continuous, periodic (with period τ) and even about $x = 0$. Hence, the Hamiltonian has point-symmetry centres at $x = A_n = n\tau$ and $x = B_n = n\tau + \tau/2$, with n being an integer. In the following sections, the functions with definite parity about A_n or B_n are denoted with a superscript e (even) or o (odd). For example, A_n^{o} represents functions which are odd about A_n.

The transfer matrix $T(E; x, x_0)$ depends on the energy E and connects the points x_0 and x. It satisfies $\phi(x) = T(E; x, x_0)\phi(x_0)$, where

$$\phi(x) = \begin{pmatrix} \psi(x) \\ \varphi(x) \end{pmatrix} = \begin{pmatrix} \psi(x) \\ m_0\tau\psi'(x)/m^*(x) \end{pmatrix} \tag{3}$$

is a continuous function [5], with m_0 being the electron mass. This matrix may be written as [16] $T(E;x,x_0)=\Lambda(x)\Lambda^{-1}(x_0)$, where

$$\Lambda(x)=\begin{pmatrix}\psi_1(x) & \psi_2(x)\\ \varphi_1(x) & \varphi_2(x)\end{pmatrix}, \tag{4}$$

with $\psi_1(x)$ and $\psi_2(x)$ being linearly independent eigenfunctions of $\hat{H}$ for the energy E. Hence, the Wronskian $W(x)=|\Lambda(x)|$ is independent of x, and consequently $|T(E;x,x_0)|=W(x)/W(x_0)=1$. It is also worth noting that $T(E;x,x_0)$ is a real and continuous function of both x and x_0, and that a nontrivial solution $\phi(x)$ does not vanish anywhere, since $\phi(x_0)=0$ leads to $\phi(x)\equiv 0$.

In particular, when $x=x_0$ is an inversion centre of the crystal (an A_n or B_n point for the Hamiltonian (2)), the functions $\psi_1(x)$ and $\psi_2(x)$ may be conveniently chosen to satisfy [2]

$$\Lambda(x_0)=\begin{pmatrix}1 & 0\\ 0 & 1\end{pmatrix}. \tag{5}$$

Hence, $T(E;x,x_0)=\Lambda(x)$ and $\psi_1(x)$ [$\psi_2(x)$] is even [odd] about $x=x_0$.

3. Minibands and minigaps

The transfer matrix technique is suitable to deal with Bloch states in one dimension [16]. In fact, the dispersion relation $E_{j,k}$ may be found as the jth root of

$$\cos(k\tau)=\mu(E)\equiv\tfrac{1}{2}\operatorname{Tr}(M(E)), \tag{6}$$

with $M(E)=T(E;\tau/2,-\tau/2)$, since $\phi_k(\tau/2)=M(E)\phi_k(-\tau/2)$ and

$$\phi_k(\tau/2)=\exp(\mathrm{i}k\tau)\phi_k(-\tau/2). \tag{7}$$

Equation (6) indicates that one may limit the analysis to $0\leqslant k\leqslant\pi/\tau$, since $E_{j,-k}=E_{j,k}=E_{j,k+2\pi/\tau}$, and that $\mu(E)$ determines the band structure. In fact [2], the function $\mu(E)$ is analytic, tends to $+\infty$ as $E\to-\infty$, and oscillates as energy increases with local minima (maxima) which are never greater (less) than -1 (1). Hence, the band structure consists of an infinite sequence of minibands separated by minigaps, with edge states at $k=0$ and π/τ (Γ and X points of the Brillouin zone, respectively).

Due to the inversion symmetry of the 1D crystal, we consider Bloch states with definite parity about $x=0$. Such functions correspond to [15] $k=0$ and π/τ, as derives from equation (7) and the condition $\phi_k(\tau/2)\neq 0$. In fact, an A_0^{e} BF satisfies

$$\begin{pmatrix}\psi_k(\tau/2)\\ \varphi_k(\tau/2)\end{pmatrix}=\exp(\mathrm{i}k\tau)\begin{pmatrix}\psi_k(\tau/2)\\ -\varphi_k(\tau/2)\end{pmatrix}, \tag{8}$$

which leads to $k=0$ and $\varphi_k(\tau/2)=0$ ($k=\pi/\tau$ and $\psi_k(\tau/2)=0$) if $\psi_k(\tau/2)\neq 0$ [$\varphi_k(\tau/2)\neq 0$]. The situation is similar for A_0^{o} BFs. Furthermore, $\psi_0(x)$ [$\psi_{\pi/\tau}(x)$] has the same parity [opposite parities] about A_0 and B_0. Thus, there are four types of edge states: each $\psi_0(x)$ has Γ_1 (A_0^{e} and B_0^{e}) or Γ_2 (A_0^{o} and B_0^{o}) symmetry and each $\psi_{\pi/\tau}(x)$ has X_1 (A_0^{e} and B_0^{o}) or X_2 (A_0^{o} and B_0^{e}) symmetry.

With this classification, equations for the energy of edge states derive from

$$\phi_k(\tau/2)=S(E)\phi_k(0) \tag{9}$$

and $\phi_k(0)\neq 0$, where $S(E)=T(E;\tau/2,0)$. Namely, a Γ_1 state fulfils

$$\begin{pmatrix}\psi_0(\tau/2)\\ 0\end{pmatrix}=\begin{pmatrix}S_{11} & S_{12}\\ S_{21} & S_{22}\end{pmatrix}\begin{pmatrix}\psi_0(0)\\ 0\end{pmatrix}, \tag{10}$$

thus leading to $S_{21} = 0$. In this way, equations

$$S_{21}(E) = 0, \qquad S_{12}(E) = 0, \qquad S_{11}(E) = 0 \qquad \text{and} \qquad S_{22}(E) = 0, \tag{11}$$

hold, for Γ_1, Γ_2, X_1 and X_2 states respectively.

The matrix $S(E)$ may also be used to obtain a whole MB, because it is closely related to $M(E)$. In fact, due to symmetry,

$$R(E) = T(E; -\tau/2, 0) = \begin{pmatrix} S_{11} & -S_{12} \\ -S_{21} & S_{22} \end{pmatrix}, \tag{12}$$

and the relation is

$$M(E) = S(E)R^{-1}(E) = \begin{pmatrix} S_{11}S_{22} + S_{21}S_{12} & 2S_{11}S_{12} \\ 2S_{22}S_{21} & S_{11}S_{22} + S_{21}S_{12} \end{pmatrix}. \tag{13}$$

Moreover, equation (6) leads to

$$\mu(E) = S_{11}S_{22} + S_{21}S_{12} = 1 + 2S_{21}S_{12} = 2S_{11}S_{22} - 1, \tag{14}$$

since $|S(E)| = S_{11}S_{22} - S_{21}S_{12} = 1$. Thus, as a generalization of previous approaches to the KP model [17–19], the secular equation (6) may be rewritten as

$$\cos^2(k\tau/2) = S_{11}S_{22} \qquad \text{or} \qquad \sin^2(k\tau/2) = -S_{21}S_{12}. \tag{15}$$

Furthermore, allowed states fulfil

$$\sin^2(k\tau) = -4S_{11}(E_k)S_{12}(E_k)S_{22}(E_k)S_{21}(E_k) = -M_{12}(E_k)M_{21}(E_k), \tag{16}$$

which comes from equations (13) and (15), but derives from (6), (13) and $|M(E)| = 1$ as well.

From equation (6) and the properties of $\mu(E)$, the edge states occur at k-values in the period-four sequence [2] (Γ, X, X, Γ, Γ, X, X, Γ, ...) as energy increases. Here, the $2j - 1$ and $2j$ ($2j$ and $2j + 1$) elements give the edges of the jth MB (minigap). In particular, the first element corresponds to the lower edge of the first MB. This state has Γ_1 symmetry, since the ground state has no nodes. However, the parity of other edge BFs is not known *a priori*. In other words, edge states of a finite minigap at Γ (X) have opposite parities but, in general, the symmetry of the lower one may be either Γ_1 or Γ_2 (X_1 or X_2). Thus, according to the parity, the following four classes of simple MB are considered [2]: Γ_1–X_1, Γ_2–X_2, Γ_1–X_2 and Γ_2–X_1.

A null minigap may occur for $k = 0$ or π/τ at a degenerate energy E satisfying [2] $\mu(E) = \pm 1$ and $\mu'(E) = 0$. Since two linearly independent states with opposite parities are allowed for such an energy, the conditions for an NMG read

$$S_{21}(E) = S_{12}(E) = 0 \qquad \text{and} \qquad S_{11}(E) = S_{22}(E) = 0 \tag{17}$$

for Γ and X respectively.

4. Bloch–Kohn functions

4.1. Phase choice

As pointed out above, the complex phase of BFs should be appropriately chosen to give WKFs. Hence, BFs are considered as analytic functions of k satisfying (a) periodicity in the reciprocal space [20] $\psi_{k+2\pi/\tau}(x) = \psi_k(x)$, (b) $\psi_{-k}(x) = \psi_k^*(x)$, which guarantees the WFs to be real, and (c) a symmetry condition which depends on the MB class. Namely [12], a Γ_1–X_1, Γ_2–X_2, Γ_1–X_2 or Γ_2–X_1 MB requires $\psi_{-k}(x) = \psi_k(-x)$, $\psi_{-k}(x) = -\psi_k(-x)$, $\psi_{-k}(x) = \psi_k(\tau - x)$

Table 1. Phase choice for BKFs $\psi_k(x)$ of each MB class, with $\alpha_k = \mathrm{i}\sin(k\tau)/2$ and $\beta_k = \pi\hbar^2\mu'(E_k)/(m_0\tau^2)$. The symmetry of the corresponding WKFs $w(x)$ is also given.

MB	$\psi_k(0)$	$\varphi_k(0)$	$w(x)$
Γ_1–X_1	$(-S_{12}S_{22}/\beta_k)^{1/2}$	$\alpha_k\psi_k(0)/(S_{12}S_{22})$	A_0^{e}
Γ_2–X_2	$\alpha_k\varphi_k(0)/(S_{21}S_{11})$	$(S_{21}S_{11}/\beta_k)^{1/2}$	A_0^{o}
MB	$\psi_k(\tau/2)$	$\varphi_k(\tau/2)$	$w(x)$
Γ_1–X_2	$(-S_{11}S_{12}/\beta_k)^{1/2}$	$\alpha_k\psi_k(\tau/2)/(S_{11}S_{12})$	B_0^{e}
Γ_2–X_1	$\alpha_k\varphi_k(\tau/2)/(S_{22}S_{21})$	$(S_{22}S_{21}/\beta_k)^{1/2}$	B_0^{o}

or $\psi_{-k}(x) = -\psi_k(\tau - x)$ respectively. Correspondingly, $\psi_k(0)$, $\varphi_k(0)$, $\psi_k(\tau/2)$ or $\varphi_k(\tau/2)$ is chosen as positive for all k, and is determined from the normalization condition [2]

$$\int_{-\tau/2}^{\tau/2} |\psi_k(x)|^2 \,\mathrm{d}x = \frac{\hbar^2\mu'(E_k)}{2m_0\tau} N_k = \frac{\tau}{2\pi}, \tag{18}$$

with

$$N_k = -\frac{|\psi_k(0)|^2}{S_{12}(E_k)S_{22}(E_k)}. \tag{19}$$

In fact, as equation (7) may be rewritten as

$$S(E_k)\phi_k(0) = \exp(\mathrm{i}k\tau)R(E_k)\phi_k(0), \tag{20}$$

one obtains

$$R^{-1}(E_k)S(E_k)\phi_k(0) = \begin{pmatrix} \cos(k\tau) & 2S_{12}S_{22} \\ 2S_{21}S_{11} & \cos(k\tau) \end{pmatrix} \phi_k(0) = \exp(\mathrm{i}k\tau)\phi_k(0), \tag{21}$$

and

$$\psi_k(0) = \frac{\mathrm{i}\sin(k\tau)}{2S_{21}(E_k)S_{11}(E_k)}\varphi_k(0). \tag{22}$$

Moreover, equations (9), (15) and (22) lead to

$$\psi_k(\tau/2) = S_{11}\psi_k(0) + S_{12}\varphi_k(0) = \frac{\mathrm{i}\sin(k\tau/2)\exp(\mathrm{i}k\tau/2)}{S_{21}(E_k)}\varphi_k(0), \tag{23}$$

then

$$\psi_k(0) = \frac{\cos(k\tau/2)\exp(-\mathrm{i}k\tau/2)}{S_{11}(E_k)}\psi_k(\tau/2). \tag{24}$$

Similarly, one obtains

$$\psi_k(0) = \frac{\mathrm{i}\sin(k\tau/2)\exp(-\mathrm{i}k\tau/2)}{S_{21}(E_k)}\varphi_k(\tau/2). \tag{25}$$

Hence, equations (15), (16), (19), (22), (24) and (25) lead to

$$N_k = \frac{|\varphi_k(0)|^2}{S_{21}(E_k)S_{11}(E_k)} = -\frac{|\psi_k(\tau/2)|^2}{S_{11}(E_k)S_{12}(E_k)} = \frac{|\varphi_k(\tau/2)|^2}{S_{22}(E_k)S_{21}(E_k)}. \tag{26}$$

Accordingly, table 1 displays the phase choice for the different MB classes, and allows a direct calculation of normalized BKFs by the transfer matrix technique. Then, WKFs may be obtained by equation (1).

To illustrate the relevance of the present phase choice, we consider the WFs of a 'diatomic' SL. Although such states have been studied in some detail [9], the phase of Bloch states has

been chosen in a way (see equation (15) of [9]) that does not always lead to exponentially localized Wannier states (see top panels in figures 4 and 5 of [9]). In particular, the first-MB WF, which is associated with the 'ground molecular orbital', is centred at the origin and poorly localized when the 'intermolecular' barriers are thinner than the 'intramolecular' ones. Unexpectedly, this result has been interpreted as due to a single-atom regime [9]. Indeed, such a configuration corresponds to another 'dimer lattice', where the 'molecules' are separated by the wider barriers, and hence the corresponding first-MB WKF should not be centred at the origin.

4.2. Symmetry

Due to the phase choice above, the real and imaginary parts of BKFs have opposite parities [21]. In particular, $\mathrm{Re}(\psi_k)$ is of A_0^{e}, A_0^{o}, B_0^{e} or B_0^{o} type for a Γ_1–X_1, Γ_2–X_2, Γ_1–X_2 or Γ_2–X_1 MB respectively. Consequently, BKFs have mixed parities in general [15]. The effective parity of $\psi_k(x)$ about $x = x_0$ with radius $n\tau + \tau/2$ is given by the scalar product

$$P_k^{(n)}(x_0) = \frac{2\pi}{(2n+1)\tau} \int_{-n\tau-\tau/2}^{n\tau+\tau/2} \psi_k^*(x_0 + x)\psi_k(x_0 - x)\,\mathrm{d}x = f_n(k) P_k^{(0)}(x_0), \tag{27}$$

where

$$f_n(k) = \begin{cases} 1, & \text{for integer } k\tau/\pi \\ \dfrac{\sin((2n+1)k\tau)}{(2n+1)\sin(k\tau)}, & \text{otherwise.} \end{cases} \tag{28}$$

Note that $P_k^{(n)}(x_0)$ equals 1 (-1) if $\psi_k(x)$ is even (odd) about $x = x_0$, and lies between -1 and 1 otherwise. Of course, this effective parity is independent of the phase choice and gives local information which, due to $f_n(k)$, is independent of the radius in special cases only. Furthermore, according to the linear dependence of $\psi_k(x)$, $\psi_{-k}^*(x)$ and $\psi_{k+2\pi/\tau}(x)$, it follows that $P_k^{(n)}(x_0) = P_{-k}^{(n)}(x_0) = P_{k+2\pi/\tau}^{(n)}(x_0)$.

5. Wannier–Kohn functions

5.1. Symmetry

The symmetry conditions associated with the phase choice above determine the symmetry of WKFs. In fact, according to equation (1), $\psi_{-k}(x) = \pm\psi_k(-x)$ and $\psi_{-k}(x) = \pm\psi_k(\tau - x)$ lead to $w(-x) = \pm w(x)$ and $w(\tau - x) = \pm w(x)$ respectively [2]. Hence, the symmetry centre of $w(x)$, which may be found as

$$\langle x \rangle = \frac{2\pi}{\tau} \int_{-\infty}^{+\infty} x|w(x)|^2\,\mathrm{d}x, \tag{29}$$

equals A_0 or B_0. Moreover, $w(x)$ is even (odd) about $x = 0$ for a Γ_1–X_1 (Γ_2–X_2) MB, and is even (odd) about $x = \tau/2$ for a Γ_1–X_2 (Γ_2–X_1) MB. Therefore, in agreement with table 1, $w(x - n\tau)$ may be classified as A_n^{e}, A_n^{o}, B_n^{e} or B_n^{o}.

It is also worth noticing that the coordinate shift $x \to x + \tau/2$ leads to $A_n \to B_n$ and $B_n \to A_{n+1}$. Correspondingly, the symmetry X_1 becomes X_2 and vice versa. Thus, the symmetry notations change with this shift, but the actual properties of BKFs and WKFs remain the same. In particular, the symmetry centres of the WKFs for a given MB, which are the Wyckoff positions [4], are independent of the coordinate system.

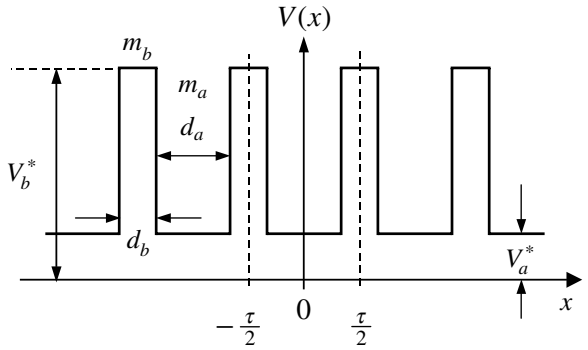

Figure 1. A few periods of the effective potential and mass profiles of the KP model for the SLs under investigation.

5.2. Localization

As stated above, WKFs are exponentially localized. In fact, the coefficient of such a decay for the jth MB is found as [2]

$$\bar{h}_j = \begin{cases} h_1, & \text{if } j = 1 \\ \min(h_j, h_{j-1}), & \text{if } j > 1, \end{cases} \tag{30}$$

where

$$h_j = \frac{1}{\tau} \ln\Big(|\mu(E_j)| + \sqrt{\mu^2(E_j) - 1}\Big), \tag{31}$$

with E_j being the jth zero of $\mathrm{d}\mu/\mathrm{d}E$. Moreover, the decay of WKFs has been shown to be faster than pure exponential, as due to a power-law prefactor [3]. In fact, $w_j(x)$ presents an oscillatory behaviour which is modulated by the function

$$v_j(x) = |x - \langle x\rangle_j|^{-3/4} \exp(-\bar{h}_j|x - \langle x\rangle_j|). \tag{32}$$

Note that the term $\langle x\rangle_j$, as given by equation (29), allows $v_j(x)$ to have the same symmetry centre as $w_j(x)$.

6. Kronig–Penney model

6.1. Theory

The KP model has been successfully used to study electron states within the effective-mass approximation in periodic a–b SLs [5, 13], where a and b represent layers of widths d_a and d_b. The period of such SLs is $\tau = d_\mathrm{a} + d_\mathrm{b}$, and the origin of coordinates is conveniently chosen at the midpoint of an a-layer. Hence, a 1D problem along the SL growth direction (x-axis), as described by equation (2), is obtained for each in-plane wavenumber $\vec{q}$. As shown in figure 1, $V(x)$ is $V_\mathrm{a}^* = V_\mathrm{a} + \hbar^2 q^2/(2m'_\mathrm{a})$ [$V_\mathrm{b}^* = V_\mathrm{b} + \hbar^2 q^2/(2m'_\mathrm{b})$] for $|x| \leqslant d_\mathrm{a}/2$ [$d_\mathrm{a}/2 < |x| < \tau/2$], where V_a and V_b give the conduction-band bottom energies in layers a and b respectively. Moreover, m_a and m_b (m'_a and m'_b) are the corresponding longitudinal (in-plane) effective-mass values. Therefore, the matrix $S(E) = T(E; \tau/2, d_\mathrm{a}/2)T(E; d_\mathrm{a}/2, 0)$ may be easily derived as

$$S(E) = \begin{pmatrix} c_\mathrm{a}c_\mathrm{b} - \frac{m_\mathrm{b}k_\mathrm{a}}{m_\mathrm{a}k_\mathrm{b}} s_\mathrm{a}s_\mathrm{b} & \frac{1}{m_0\tau}\left(\frac{m_\mathrm{a}}{k_\mathrm{a}} c_\mathrm{b}s_\mathrm{a} + \frac{m_\mathrm{b}}{k_\mathrm{b}} c_\mathrm{a}s_\mathrm{b}\right) \\ -m_0\tau\left(\frac{k_\mathrm{a}}{m_\mathrm{a}} c_\mathrm{b}s_\mathrm{a} + \frac{k_\mathrm{b}}{m_\mathrm{b}} c_\mathrm{a}s_\mathrm{b}\right) & c_\mathrm{a}c_\mathrm{b} - \frac{m_\mathrm{a}k_\mathrm{b}}{m_\mathrm{b}k_\mathrm{a}} s_\mathrm{a}s_\mathrm{b} \end{pmatrix}, \tag{33}$$

where $c_r = \cos(k_r d_r/2)$, $s_r = \sin(k_r d_r/2)$ and $k_r = (2m_r(E - V_r^*)/\hbar^2)^{1/2}$, with r being a or b. Furthermore, equation (14) leads to the well-known expression [5]

$$\mu(E) = \cos(k_a d_a)\cos(k_b d_b) - \frac{1}{2}\left(\frac{m_b k_a}{m_a k_b} + \frac{m_a k_b}{m_b k_a}\right)\sin(k_a d_a)\sin(k_b d_b). \quad (34)$$

Hence, an NMG requires

$$\frac{2(V_b^* - V_a^*)}{\pi^2\hbar^2} = \frac{n_a^2}{m_a d_a^2} - \frac{n_b^2}{m_b d_b^2} \quad (35)$$

or

$$\frac{2(V_b^* - V_a^*)}{\pi^2\hbar^2} = \frac{(m_a - m_b)p^2}{(m_a d_a + m_b d_b)^2}, \quad (36)$$

where n_a, n_b and p are nonnegative integers. In fact, according to equations (17) and (33), an NMG at X leads to a linear system of equations for the variables $c_a c_b$ and $s_a s_b$, with determinant $m_b k_a/(m_a k_b) - m_a k_b/(m_b k_a)$. A nonvanishing determinant leads to (35), whereas (36) holds otherwise. The same reasoning applies to the Γ point, but NMGs at Γ (X) occur for even (odd) values of $n_a - n_b$ and p.

When $k_a d_a = n_a\pi$ and $k_b d_b = n_b\pi$ the equation (35) applies, and an NMG occurs due to hybridization of separate layer resonances [14], which is herein called a type-I degeneration. Otherwise, the occurrence of an NMG should be due to a type-II degeneration, which requires $k_a = p\pi m_a/(m_a d_a + m_b d_b)$, $k_b = p\pi m_b/(m_a d_a + m_b d_b)$ and equation (36). This second type of NMG is due the position dependence of the longitudinal effective mass [19] and, according to equation (36), requires $(V_b^* - V_a^*)(m_a - m_b) \geqslant 0$. Moreover, both types of degeneration require k_a and k_b to be real, hence NMGs are allowed for energies above the barrier height $\max(V_a^*, V_b^*)$ only [17].

6.2. Numerical results

To fix ideas, conduction states with in-plane momentum $q = 0$ in $Al_{0.48}In_{0.52}As$–$Ga_{0.47}In_{0.52}As$ SLs are considered [14]. Such systems are herein labelled as SL1, and their parameters are $m_a = 0.043\,m_0$, $m_b = 0.070\,m_0$, $V_a = 0$ eV, $V_b = 0.51$ eV, $d_b = 88.0$ Å and d_a (to be varied).

The lower four MBs and minigaps are plotted as functions of d_a in figure 2, where the edge energies are solutions of equations (11) and correspond to Bloch states with Γ_1, Γ_2, X_1 or X_2 symmetry. At first sight, the most apparent characteristics of the spectrum are the existence of NMGs and the corresponding serrated edges of MBs. Such NMGs are explained as type-I degenerations at $E = V_b + \hbar^2\pi^2 n_b^2/(2m_b d_b^2)$, since $q = 0$, $V_b > V_a$ and $m_a < m_b$ contradict equation (36). In fact, as displayed in figure 2, the first minigap (at X) is everywhere finite, while the second (at Γ) vanishes for $d_a = 38.9$ Å (with $n_a = n_b = 1$). Also, the third minigap (at X) closes for $d_a = 33.3$ Å (with $n_a = 1$ and $n_b = 2$) and $d_a = 77.7$ Å (with $n_a = 2$ and $n_b = 1$). It is very interesting to note that the minigap edge states interchange their parities when the minigaps vanish and reopen as the d_a increases. Such behaviour is of most importance in optical studies, as discussed below. Hence, we emphasize that, in clear contrast with a previous work [7], the parity of edge states does not alternate in general, neither at Γ nor at X.

The symmetry of WKFs may be determined by inspection of figure 2. Namely, the symmetry of edge states is indicated by the different line styles, and the symmetry of WKFs is given in table 1 for each MB class. For instance, $w_1(x)$ is A_0^e for all d_a because the bottom (top) state of the first MB is Γ_1 (X_1) everywhere. In the same way, $w_2(x)$ is B_0^e for $d_a < 38.9$ Å and A_0^o for $d_a > 38.9$ Å, whereas $w_3(x)$, which is B_0^o for $d_a < 33.3$ Å, changes its symmetry as

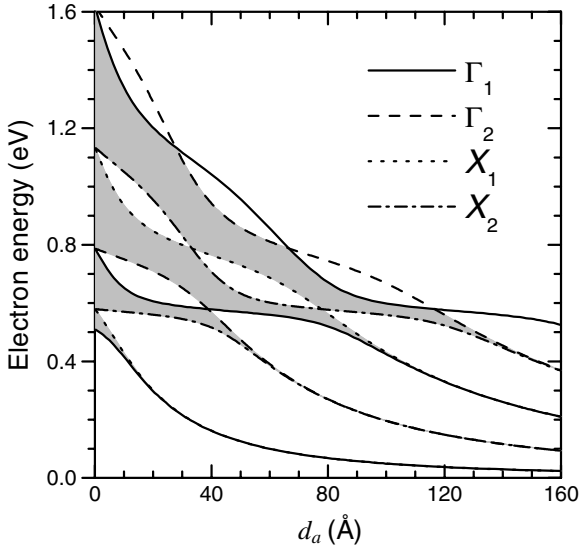

Figure 2. The lower four MBs and minigaps for SL1 as functions of the layer width d_a. Solid, dotted, dashed and dotted–dashed curves represent Γ_1, Γ_2, X_1 and X_2 edge states respectively. The shaded regions correspond to MBs.

d_a increases. In fact, $w_3(x)$ becomes A_0^o (B_0^e) after $d_a = 33.3$ Å ($d_a = 38.9$ Å), and is A_0^e for $d_a > 77.7$ Å.

It is also interesting to consider the symmetry of $w_j(x)$ for $j = 1, \ldots, 4$. On the one hand, the symmetries are A_0^e, A_0^o, A_0^e and A_0^o for $d_a > 116.6$ Å, because in the tight-binding regime the four MBs lie below the barrier, where the parities of BFs alternate. On the other hand, the symmetries are A_0^e, B_0^e, B_0^o and B_0^e for $d_a < 27.8$ Å, since this regime resembles the negative Dirac-comb potential [11]. Moreover, other sequences of symmetry occur for intermediate regimes. In particular, the parities are A_0^e, A_0^o, B_0^e, A_0^e when 66.6 Å $< d_a < 77.7$ Å. Hence, the prediction about WKFs of continuum MBs, in the sense that they would be centred at the barrier midpoint [11], is not accurate. In fact, the function $w_4(x)$, which corresponds to energies above $V_b = 0.51$ eV, is even about the well midpoint.

For a more detailed analysis of Bloch and Wannier states we now consider the system SL1 with $d_a = 50.0$ Å. The lower four MBs are shown in figure 3, where the symmetry of edge states is indicated. Hence, the first and second (third and fourth) MBs are below (above) the barrier, and are classified as Γ_1–X_1 and Γ_2–X_2 (Γ_1–X_2 and Γ_2–X_1), respectively. This classification may be confirmed in figure 4, where the effective parity of BKFs about the symmetry centres A_0 and B_0 is plotted as a function of the wavenumber k. To do so, one should remember that $P_k^{(0)}(x_0)$ is 1 (-1) when $\psi_k(x)$ is even (odd) about $x = x_0$. Moreover, figure 4 clearly shows that $\psi_0(x)$ [$\psi_{\pi/\tau}(x)$] has the same parity [opposite parities] about A_0 and B_0.

The WKFs for the same four MBs are plotted in figure 5, where the expected symmetries are clearly shown. Namely, the parities are A_0^e, A_0^o, B_0^e and B_0^o for $j = 1, \ldots, 4$, in agreement with table 1 and the classification of MBs in figure 3. Moreover, the localized nature of WKFs is apparent in figure 5, but its exponential character [2] is better shown in figure 6, where the overall linear behaviour of $\ln|w_j(x)|$ (grey dots) represents the exponential decay of $w_j(x)$. As given by equation (31), the approximate slopes in figures 6(a)–(d) are 6.34, 1.57, 0.90,

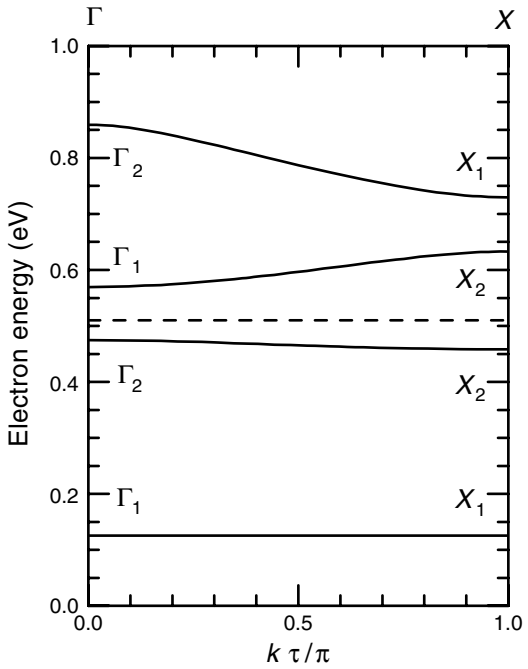

Figure 3. Dispersion relations of the lower four MBs for SL1 with $d_a = 50.0$ Å. The symmetry of edge states is indicated as Γ_1, Γ_2, X_1 or X_2, and the dashed line corresponds to the barrier height.

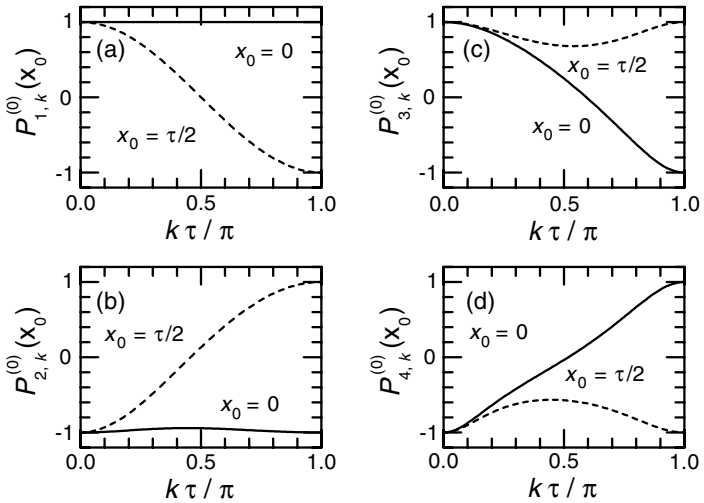

Figure 4. Effective parity $P^{(0)}_{j,k}(x_0)$ of BFs about $x_0 = 0$ (solid curve) and $x_0 = \tau/2$ (dashed curve) as a function of the wavenumber k, for SL1 with $d_a = 50.0$ Å. The parts (a)–(d) correspond to MBs 1–4 respectively.

and 0.62 respectively. Furthermore, the modulating functions $\ln|v_j(x)|$ (see equation (32)) are shown as thin solid curves in figure 6. This illustrates the expected decay of WKFs [3], where the power-law prefactor may be seen as a slight curvature in the approximate linearity of $\ln|v_j(x)|$.

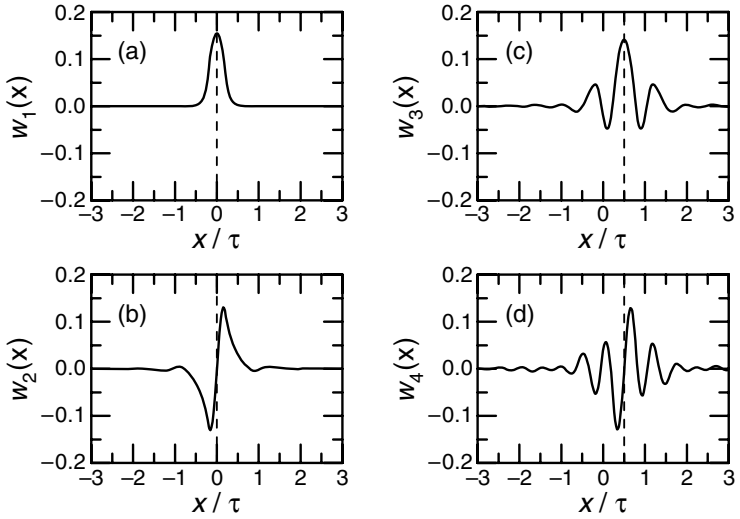

Figure 5. The WKFs of the lower four MBs for SL1 with $d_a = 50.0$ Å. The dashed lines indicate the symmetry centres.

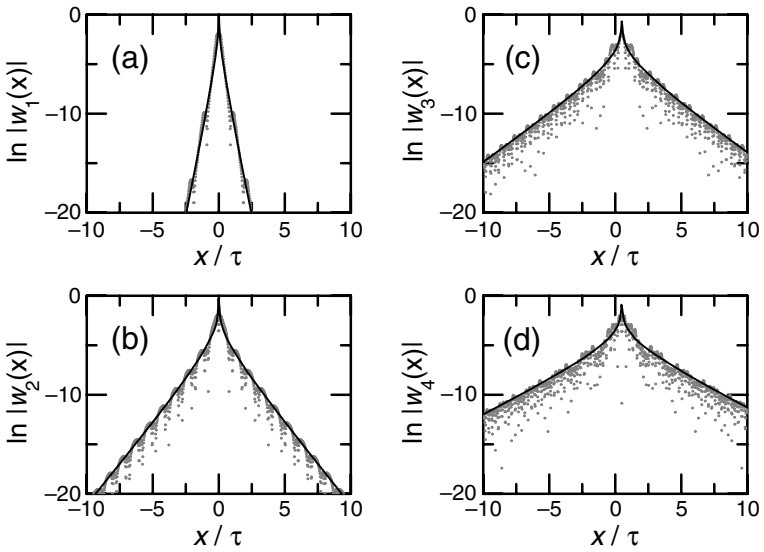

Figure 6. Natural logarithm of the WKFs (grey dots) and their modulating functions (thin solid curve) for the lower four MBs in SL1 with $d_a = 50.0$ Å.

6.3. Optical absorption

The occurrence of NMGs and parity swaps is relevant in optical studies of SLs. Namely, for light polarized along the SL axis, allowed intraband transitions occur between states with the same wavenumber $(k, \vec{q})$. However, due to symmetry, the vertical transitions between states of the same parity are forbidden. Moreover, although the finite width of MBs, where Bloch states have mixed parities, suggests a broadening of transition peaks, the higher density of states at the edge of MBs indicates that relevant peaks of absorption should be associated with

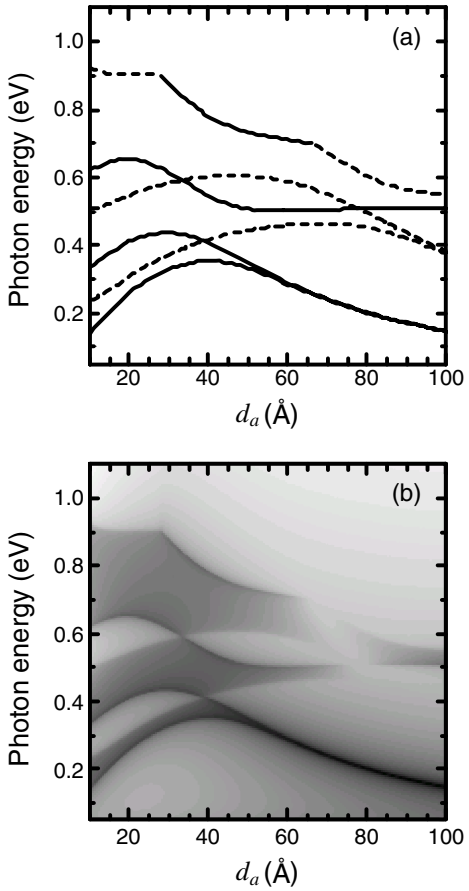

Figure 7. (a) Photon energy as a function of the well width d_a for edge-to-edge $1 \rightarrow j$ transitions in SL1. Solid (dashed) curves represent allowed $\Gamma_1 \rightarrow \Gamma_2$ and $X_1 \rightarrow X_2$ (forbidden $\Gamma_1 \rightarrow \Gamma_1$ and $X_1 \rightarrow X_1$) transitions. (b) Contour plot of the optical absorption coefficient for $1 \rightarrow j$ transitions with $j = 2, 3, 4$. The absorption values are represented in log scale and larger values are shown as darker tones.

edge states, which have definite parity. Hence, one may expect a kind of selection rule for such optical transitions.

In fact, intraband transitions in the SL1 system have been studied both theoretically and experimentally [14]. Due to the low temperature (5 K), the optical absorption is mainly due to $1 \rightarrow j$ transitions. Regarding the symmetry of edge states, the relevant transitions should be $\Gamma_1 \rightarrow \Gamma_2$ or $X_1 \rightarrow X_2$. Hence, the detected $1 \rightarrow 3$ transition near Γ for the SL1 with $d_a = 16.0$ Å (see figure 1 in [14]) should be forbidden for $d_a > 38.9$ Å (see figure 2). At the same time, the $1 \rightarrow 2$ transition near Γ should become allowed for $d_a > 38.9$ Å, as a result of the parity swap between edge states (see figure 2).

In this sense, there is no general selection rule on the MB index j for direct optical transitions involving edge states of continuum MBs in SLs [10]. Instead, one should expect absorption peaks near the energy difference between states with opposite parities in figure 2. In fact, figure 7(a) shows the photon energy as a function of the well width for edge-to-edge $1 \rightarrow j$ transitions. Solid (dashed) curves represent allowed $\Gamma_1 \rightarrow \Gamma_2$ and $X_1 \rightarrow X_2$ (forbidden $\Gamma_1 \rightarrow \Gamma_1$ and $X_1 \rightarrow X_1$) transitions. Moreover, figure 7(b) displays a contour plot

of the optical absorption coefficient for $1 \rightarrow j$ transitions with $j = 2, 3, 4$. In agreement with the theoretical and experimental work [14], the absorption coefficient of SL1 at 5 K has been computed for a conduction electron density of 5×10^{17} cm^{-3}. However, the lifetime broadening in Fermi's golden rule is taken as 5 meV, to better show the absorption peaks. Moreover, we have considered a parabolic model for the conduction band. The absorption values are represented on a log scale and larger values are shown as darker tones in figure 7(b).

At first sight, the overall agreement between panels (a) and (b) of figure 7 is apparent. Namely, the edges of the absorption bands in panel (b) are reproduced by the curves in panel (a). However, noting the most interesting result requires a careful inspection. In fact, the absorption peaks, which correspond to the darker edges of the absorption bands in panel (b), reproduce the solid curves in figure 7(a), which correspond to allowed transitions. At the same time, the dashed curves in panel (a), which represent forbidden transitions, reproduce the weaker edges of absorption bands in figure 7(b). Furthermore, the second and third absorption bands in panel (b) do not appear at well-width values for which both edges of the band correspond to forbidden transitions in panel (a).

6.4. Further results on null minigaps

Although the NMGs in SL1 are due to separate layer resonances, type-II degenerations also occur in SLs. In fact, conduction states with $q = 0$ have been studied in 50 Å-$In_{0.69}Ga_{0.31}As$/50 Å-InP nearly effective-mass SLs [8]. The first minigap was calculated as a function of V_a for $m_a = 0.034\, m_0$, $m_b = 0.073\, m_0$, $V_b = 0$ eV, and it was found to vanish at $V_a \approx 51$ meV. However, the zero-energy minigap was not successfully explained [8], since equation (5) of [8] is equivalent to equation (35) here. Actually, such an NMG corresponds to $p = 1$ in equation (36).

7. Conclusions

Bloch and Wannier functions in a 1D crystal with inversion symmetry have been considered. First, we have shown that, in general, the parity of Bloch states does not alternate as energy increases, neither at Γ nor at X. Unfortunately, this aspect has been incorrectly treated in the literature [7], maybe because localized and below-barrier states present the alternating sequence of parities. We have also set up equations for the edge levels associated with each possible symmetry and have given conditions for the occurrence of NMGs. Such zero-energy gaps and the associated interchanges of parity between edge states have been shown to be the clue to explain the lack of a general alternating sequence of parities. Also, the relation between the phase choice for Bloch states and the symmetry of WFs has been given. Moreover, we have introduced a concept of effective parity of Bloch states which is helpful in optical studies, for instance.

Additionally, we may set up a direct procedure to obtain WKFs. First, the MBs are classified according to the symmetry of their edge states. The classification of the lower J MBs follows three stages:

(i) find the lower $1 + [J/2]$, $[J/2]$, $[(J + 1)/2]$ and $[(J + 1)/2]$ zeros of $S_{21}(E)$, $S_{12}(E)$, $S_{11}(E)$ and $S_{22}(E)$ respectively[3];
(ii) sort the corresponding symmetries Γ_1, Γ_2, X_1 and X_2 as energy increases and drop the last term;
(iii) associate neighbour terms into pairs and get the desired classes.

[3] Here $[x]$ represents the larger integer which is not larger than x.

Next, the dispersion relations $E_{j,k}$ are found in the energy ranges supplied by the classification procedure for a k-mesh with $0 \leqslant k \leqslant \pi/\tau$. Last, the normalized Bloch states are obtained from table 1 by the transfer matrix technique, and the WFs are calculated through equation (1) by numerical integration. Of course, this procedure applies whenever NMGs do not occur, thus leading to a set of simple MBs [2].

We have applied the developed theory to the KP model. Explicit conditions for NMGs have been derived. In this sense, it is important to stress that two types of degeneration were found. The first type is well known and consists of separate layer resonances [14], while the second has been previously considered for effective-mass SLs only [19]. In particular, we have identified type-II degenerations in nearly effective-mass SLs [8]. Furthermore, we have discussed the effects of NMGs and parity swaps on the optical properties of semiconductor SLs. In this respect, we have found that no general selection rule applies to the MB index j for intraband transitions between edge states.

Finally, we expect our theory to clarify various aspects of the subject, and to be useful in the study of systems such as compound-period SLs [9, 13]. Applications of this approach to the calculation of localized states in SLs, the study of additional 1D models and extensions to noncentrosymmetric crystals and composite MBs are in progress.

Acknowledgments

This work was supported by the Brazilian Agencies FAPESP and FUNDUNESP. We are grateful to F M Peeters, P P Gonzalez-Borrero, M E Mora-Ramos and A S Florêncio for useful discussions. ABA is thankful to IFSC-USP for hospitality.

References

[1] Wannier G H 1959 *Elements of Solid State Theory* (New York: Cambridge University Press)
[2] Kohn W 1959 *Phys. Rev.* **115** 809
[3] He L and Vanderbilt D 2001 *Phys. Rev. Lett.* **86** 5341
[4] Marzari N and Vanderbilt D 1997 *Phys. Rev.* B **56** 12847 and references therein
[5] Bastard G 1981 *Phys. Rev.* B **24** 5693
[6] Wacker A 2002 *Phys. Rep.* **357** 1
[7] Cho H-S and Prucnal P R 1987 *Phys. Rev.* B **36** 3237
[8] Kucharczyk R and Steślicka M 1997 *Vacuum* **48** 241
[9] Guerrero H M, Cocoletzi G H and Ulloa S E 1995 *J. Appl. Phys.* **78** 2541
[10] Gershoni D, Oiknine-Schlesinger J, Ehrenfreund E, Ritter D, Hamm R A and Panish M B 1993 *Phys. Rev. Lett.* **71** 2975
[11] Pedersen F B, Einevoll G T and Hemmer P C 1991 *Phys. Rev.* B **44** 5470
[12] Smirnov V P and Usvyat D E 1999 *Phys. Rev.* B **59** 9695
[13] Peeters F M and Vasilopoulos P 1989 *Appl. Phys. Lett.* **55** 1106
[14] Sirtori C, Capasso F, Sivco D L and Cho A Y 1994 *Appl. Phys. Lett.* **64** 2982
[15] Pan S-H and Feng S-M 1991 *Phys. Rev.* B **44** 5668
[16] Mora M E, Pérez R and Sommers Ch B 1985 *J. Physique* **46** 1021
[17] Folland N O 1983 *Phys. Rev.* B **28** 6068
[18] Allen G 1953 *Phys. Rev.* **91** 531
[19] Milanović V and Ikonić Z 1988 *Phys. Rev.* B **37** 7125
[20] Bulyanitsa D S and Svetlov Yu E 1962 *Sov. Phys.—Solid State* **4** 981
[21] Glutsch S 1999 *J. Phys.: Condens. Matter* **11** 5533